Atomistic modeling of radiation-induced disordering and dissolution at a Ni/Ni_3Al interface

Tongsik Lee[a)]
Department of Materials Science and Engineering, Massachusetts Institute of Technology, Massachusetts 02139, USA
Alfredo Caro
Materials Science and Technology Division, Los Alamos National Laboratory, New Mexico 87545, USA
Michael J. Demkowicz
Department of Materials Science and Engineering, Massachusetts Institute of Technology, Massachusetts 02139, USA

(Received 22 September 2014; accepted 25 November 2014)

$L1_2$-ordered γ' precipitates embedded in a fcc γ matrix impart excellent mechanical properties to nickel-base superalloys. However, these enhanced mechanical properties are lost under irradiation, which causes the γ' precipitates to disorder and dissolve. We conduct an atomic-level study of radiation-induced disordering and dissolution at a coherent (100) facet of an initially ordered γ' Ni_3Al precipitate neighboring a pure Ni γ matrix. Using molecular dynamics, we simulate collision-induced events by sequentially introducing 10 keV primary knock-on atoms with random positions and directions. In the absence of thermally assisted recovery processes, the ordered Ni_3Al layer disorders rapidly within 0.1–0.2 dpa and then gradually dissolves into the adjacent Ni layer at higher doses. Both the disordering efficiency and mixing parameter calculated from the simulations lie within the range of values found by experiments carried out at room temperature, where thermally activated diffusion is insignificant.

I. INTRODUCTION

$L1_2$-ordered intermetallic γ' precipitates embedded in a disordered fcc γ matrix impart excellent mechanical properties to nickel-base superalloys.[1] However, γ' precipitates undergo disordering and dissolution under irradiation, thereby degrading the mechanical properties of these alloys. A great deal of experimental[2–11] and theoretical[12–18] effort has been devoted to study the stability of the γ/γ' microstructure in these superalloys under irradiation. Moreover, several atomic-scale modeling studies have been carried out to elucidate the mechanisms of disordering in Ni_3Al,[19–30] which is a common γ' precipitate composition in Ni-base alloys. These mechanisms operate over picosecond-scale times, making them difficult to investigate experimentally. Nevertheless, atomic-level simulations of the disordering and dissolution processes of a γ' precipitate in a γ matrix under high-dose irradiation have not been conducted before. Such simulations are a means to connect the well-known microscopic-level mechanisms governing γ' behavior under irradiation to macroscale disordering and dissolution rates.

The aim of this study is to present an atomistic model that provides an accurate prediction of radiation-induced disordering and dissolution of γ' precipitates in a γ matrix. Following Zhang and Demkowicz,[31] we use classical potential molecular dynamics (MD) to model high-dose irradiation by sequentially simulating multiple collision cascades at a coherent interface of a γ' precipitate in a γ matrix. This approach models collision cascade-induced effects, but not thermally activated recovery. Thus, we compare our simulations to experiments carried out at room temperature, where the effect of thermally activated recovery processes is negligible. The evolution of the chemical order and dissolution of the γ' precipitate are quantified in terms of the disordering efficiency and the Averback–Peak mixing parameter.[32] We validate the simulation by comparing these values with experimental data available in the literature.[5–8,11,33,34] The disordering and dissolution rates predicted by atomistic simulations lie within the range of reported experimentally determined values.

II. SIMULATION METHOD

Several Ni-base superalloys contain cuboidal Ni_3Al γ' precipitates in a Ni-rich γ matrix.[35–37] We investigate a flat, coherent (100) facet of such precipitates in a bilayer model containing pure Ni (γ) and the stoichiometric Ni_3Al compound (γ'). The bilayer is constructed in a cubic simulation cell with edge length ~107 Å containing 108,000 atoms ($30 \times 30 \times 30$ cubic unit cells). Periodic boundary conditions (PBCs) are applied in all directions. Initially, equal parts of the simulation cell are

Contributing Editor: William J. Weber
[a)]Address all correspondence to this author.
e-mail: tongsikl@mit.edu
DOI: 10.1557/jmr.2014.377

https://doi.org/10.1557/jmr.2014.377 Published online by Cambridge University Press

filled with fcc Ni atoms and the $L1_2$-Ni_3Al intermetallic. Because of the PBCs, the model contains two Ni/Ni_3Al interfaces. The size of the simulation cell is selected to be sufficiently large so that collision cascades initiated by primary knock-on atoms (PKAs) with the recoil energy chosen for this study (10 keV) do not interact with their periodic images.

We adopt an embedded atom method (EAM)[38,39] interatomic potential developed by Mishin for the γ and γ' phases of the Ni–Al system[40] and subsequently modified by Skirlo and Demkowicz[30] to include the repulsive short-range interaction due to Ziegler et al.[41] Although there has been a more recent EAM potential developed for the Ni–Al system,[42] it has been confirmed that this potential has nearly no miscibility gap between the γ and γ' phases[43] and is therefore unsuitable for the present study. The structure of the model is equilibrated at 300 K and zero pressure using the Anderson barostat and the Nosé–Hoover thermostat[44] prior to initiating collision cascade simulations.

In the present work, we adopt the computational strategy developed by Zhang and Demkowicz in their study on radiation-induced mixing between low-solubility metals.[31] In this approach, we investigate high-dose microstructure evolution by modeling a sequence of many collision cascades. A single cascade is initiated by introducing a PKA with kinetic energy representative of subcascade energies that give rise to thermal spikes in Ni–Al alloys. For example, in Ni–Al alloys irradiated with 700 keV–6 MeV nickel ions, subcascade energies of ~10 keV are generated.[45] We therefore conduct our simulations using 10 keV PKAs. The PKA and its velocity direction are selected randomly. The model is then evolved in time under constant energy and fixed volume for ~20 ps. Time steps are dynamically adjusted during the simulation based on the atomic velocity and forces to ensure numerical accuracy.

As in previous atomistic simulations of collision cascades in crystalline metals,[46–50] PKAs in our model dissipate their kinetic energy through collisions with nearby atoms within a few tenths of a picosecond, forming molten regions several nanometers in diameter called thermal spikes (TSs). The TS subsequently cools down to near-ambient temperature and recrystallizes within the following 20 ps, leaving behind point defects and point defect clusters. At this stage, the temperature of the model is brought back to the initial ambient temperature (300 K) through a constant temperature MD simulation carried out using atomic velocity rescaling for about 10 ps.

This process is iterated approximately 3000 times in each simulation, giving a maximum dose of ~3 displacements per atom (dpa). The number of PKAs is converted to dpa by means of the modified Kinchin-Pease formula[51] with a displacement threshold energy of 40 eV.[26,52,53] Because this simulation approach corresponds to extremely high fluxes and displacement rates (~10^{27} m^{-2} s^{-1} and 10^7 dpa s^{-1} compared to ~10^{17} m^{-2} s^{-1} and 10^{-3} dpa s^{-1} in implantation experiments), it should be interpreted as modeling only non-thermally activated processes, such as ballistic mixing and TSs, rather than thermally activated ones such as Fickian diffusion, mimicking either low temperature or ultra-high flux irradiations. To obtain good statistics, each simulation is repeated 20 times with a different initial thermal equilibrium state and random number generator seed. Simulations are performed using LAMMPS[54] and the results are visualized using OVITO.[55]

We measure local chemical order using the Warren–Cowley short-range order (SRO) parameter at the second-nearest neighbor shell, $\alpha^{(2)}_{\mathrm{NiAl}}$.[56] This parameter is defined for any given Al atom as

$$\alpha^{(2)}_{\mathrm{NiAl}} = 1 - \frac{p^{(2)}_{\mathrm{NiAl}}}{m_{\mathrm{Ni}}} \quad . \tag{1}$$

Here, $p^{(2)}_{\mathrm{NiAl}}$ is the probability of finding Ni atoms in the shell and m_{Ni} is the concentration of Ni atoms of the ordered alloy. For the case of the $L1_2$-ordered Ni_3Al compound, $p^{(2)}_{\mathrm{NiAl}} = N^{(2)}_{\mathrm{NiAl}}/6$ and $m_{\mathrm{Ni}} = 3/4$, where $N^{(2)}_{\mathrm{NiAl}}$ is the number of Ni atoms in the shell. At this stoichiometry, $\alpha^{(2)}_{\mathrm{NiAl}}$ ranges from 0 to 1,with $\alpha^{(2)}_{\mathrm{NiAl}} = 0$ denoting complete disorder (i.e., a random solid solution with $p^{(2)}_{\mathrm{NiAl}} = m_{\mathrm{Ni}}$) while $\alpha^{(2)}_{\mathrm{NiAl}} = 1$ if all six second-nearest neighbors of the Al atom are other Al atoms (i.e., $N^{(2)}_{\mathrm{NiAl}} = 0$), as in the perfectly ordered $L1_2$-Ni_3Al compound. $\alpha^{(2)}_{\mathrm{NiAl}}$ may also take on negative values if the Ni concentration is more than $m_{\mathrm{Ni}} = 3/4$ in the second-nearest neighbor shell of the central Al atom.

To obtain a smooth profile of the SRO parameter as a function of position, z, perpendicular to the interfaces, we define a coarse-grained order parameter $s(z)$ as

$$s(z) = \sum_{i=1}^{N_{\mathrm{Al}}} \alpha^{(2)i}_{\mathrm{NiAl}} \exp\left(\frac{-(z-z_i)^2}{B^2}\right) \Big/ \int \mathrm{d}z \exp\left(-\frac{z^2}{B^2}\right) \quad . \tag{2}$$

Here, N_{Al} is the number of Al atoms in the system, z_i is the z-coordinate of the i-th Al atom, and B is the characteristic coarse-graining length, which is chosen to be 3 Å in the present analysis. This approach is analogous to the way smoothed composition profiles were computed in Ref. 31. We further define the average order parameter S by averaging $\alpha^{(2)}_{\mathrm{NiAl}}$ over all the Al atoms in the model.

We characterize the dissolution of the γ' precipitates using the Averback–Peak mixing parameter.[32] The dependence of the mixing parameter on the incident

https://doi.org/10.1557/jmr.2014.377 Published online by Cambridge University Press

ion energy is relatively weak, hence this parameter is a convenient measure for comparing intermixing efficiencies obtained from different experiments and simulations.[57] The mixing parameter Q has dimensions of length[5] times energy^{-1} and is defined as

$$Q = \frac{D^{\mathrm{eff}} t}{\phi F_D} \quad , \tag{3}$$

where D^{eff} is the effective interdiffusion coefficient, t is the irradiation time, ϕ is the incident particle fluence, and F_D is the nuclear stopping power (energy lost per unit distance traveled due to collisions of the incident particle with target nuclei). In our analysis, we assume that D^{eff} is independent of composition.

III. SIMULATION RESULTS

Figure 1 displays snapshots of the morphological evolution of the (100) Ni/Ni_3Al bilayer at four selected doses: 0.0, 0.04, 0.2, and 2.0 dpa, corresponding to 0, 43, 216, and 2160 PKAs, respectively. Figures 1(a)–1(d) illustrate the dissolution process of the Ni_3Al layer through intermixing of Ni (red) and Al (blue). Figures 1(e)–1(h) show only Al atoms colored by the SRO parameter [Eq. (1)]. Initially, the γ and γ' layers form sharp interfaces [Fig. 1(a)], and the Al atoms inside the γ' layer are characterized by perfect $L1_2$ order. The Al atoms at interfaces take on slightly lower values of the SRO parameter than in the bulk because of the lack of Al atoms in the γ layer [Fig. 1(e)].

As the dose increases to 0.04 dpa, the γ' phase accumulates copious antisite defects [Fig. 1(f)]. Meanwhile, the interfaces remain nearly atomically sharp due to the low levels of intermixing at this dose [Figs. 1(b) and 1(f)]. The $L1_2$ structure in the γ' layer is in effect fully destroyed by 0.2 dpa [Fig. 1(g)]. However, the interfaces still maintain their relatively sharp profiles at this dose [Figs. 1(c) and 1(g)]. At doses of 2 dpa and above, the Ni and Al atoms undergo significant mixing and the interfaces become increasingly diffuse [Figs. 1(d) and 1(h)]. The composition of the entire model is completely homogenized at higher doses.

Figure 2 shows the coarse-grained order parameter s, as a function of distance perpendicular to the interface plane, normalized by its initial value in the γ' layer, s_0. The horizontal axis in Fig. 2 corresponds to the vertical direction in the visualizations shown in Fig. 1. The normalized coarse-grained order parameter of the γ' phase, which is initially perfectly ordered, is reduced to less than a quarter of its initial value by 0.04 dpa. The value of s/s_0 for Al atoms in the core of the γ' layer approaches zero at 0.2 dpa while s/s_0 for atoms near interfaces becomes negative as the two layers interfuse.

Figure 3 shows the average order parameter S normalized by its initial value S_0 plotted as a function of dose Φ

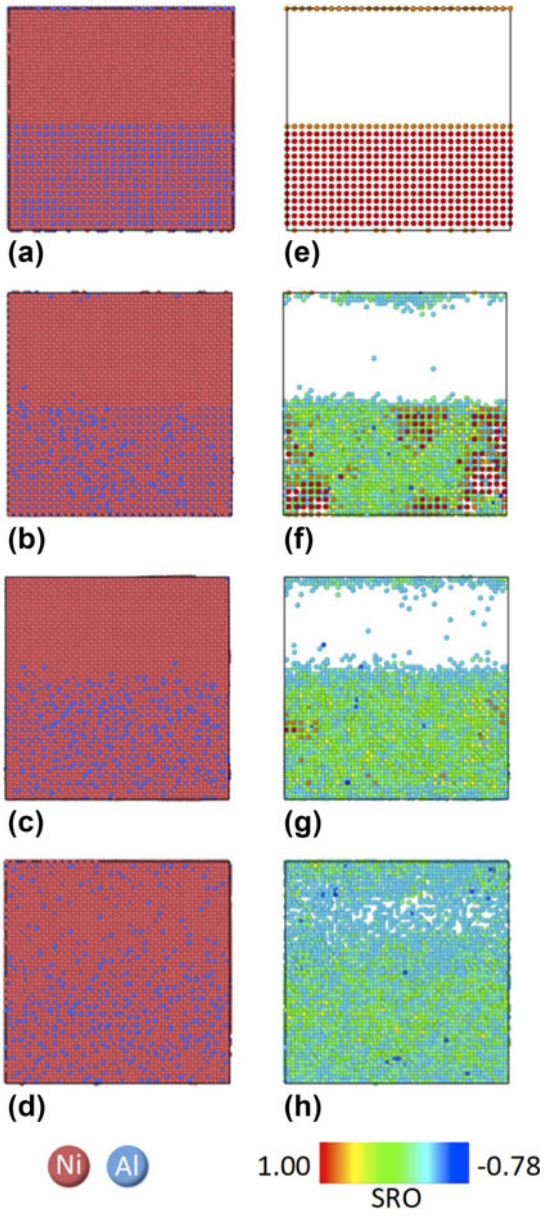


FIG. 1. Selected snapshots of the (100) Ni/Ni_3Al bilayer as a function of dose obtained from the present study. (Left column) Atoms are colored by their type (red: Ni and blue: Al) at 0.0, 0.04, 0.2, and 2.0 dpa in (a), (b), (c), and (d), respectively. (Right column) Al atoms are colored according to their SRO parameter at 0.0, 0.04, 0.2, and 2.0 dpa in (e), (f), (g), and (h), respectively.

up to 0.3 dpa for the Ni/Ni_3Al bilayer. The value of S/S_0 decays to near zero at doses as low as ~0.12 dpa. The negative asymptote of S/S_0 for the Ni/Ni_3Al bilayer is attributed to the larger proportion of Ni atoms in the model, causing a greater number of Al atoms to have negative $\alpha^{(2)}_{\mathrm{NiAl}}$ values.

Following Aronin,[58] the cascade-induced disordering at low doses may be described as a simple exponential decay

https://doi.org/10.1557/jmr.2014.377 Published online by Cambridge University Press

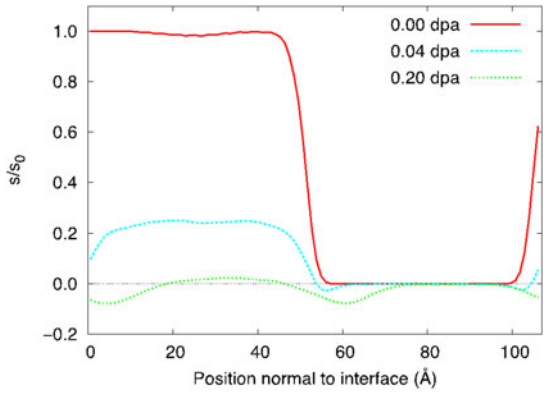


FIG. 2. Profile of the normalized coarse-grained order parameter s/s_0 plotted as a function of distance normal to Ni/Ni_3Al interfaces obtained from the present study at 0.0, 0.04, and 0.2 dpa.

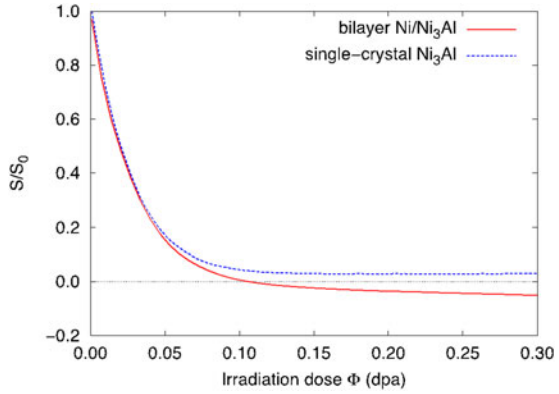


FIG. 3. Normalized average order parameter S/S_0 plotted as a function of dose for Ni_3Al single-crystal and the Ni/Ni_3Al bilayer systems obtained from the present study.

$$S = S_0 e^{-\varepsilon\Phi} \quad , \tag{4}$$

where ε is the disordering efficiency and Φ is the irradiation dose. Fitting this equation to the data in Fig. 3 yields $\varepsilon \sim 29$ dpa^{-1} for the bilayer model. This value fits within the 10–100 dpa^{-1} range reported by Russell for ion irradiation.[59]

For comparison, a plot obtained from similar calculations carried out for an initially perfectly ordered model of single-crystal Ni_3Al (i.e., a simulation cell only containing the γ′ phase) is also shown in Fig. 3. The disordering efficiency for this system is estimated to be $\varepsilon \sim 31$ dpa^{-1}, showing essentially no difference from ε for the bilayer. This result indicates that the disordering of the γ′ phase is insensitive to the presence of interfaces.

We analyze the dissolution of the γ′ layer by constructing Al concentration profiles as a function of distance perpendicular to Ni/Ni_3Al interfaces. Such profiles are shown in Fig. 4 for four selected values of irradiation dose: 0.0, 0.2, 2.0, and 3.0 dpa. Initially, the γ′ layer contains exactly 25 at.% of Al. This composition profile exhibits

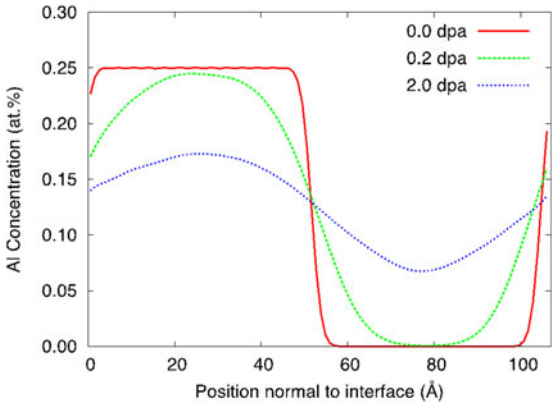


FIG. 4. Al concentration profiles as a function of distance normal to Ni/Ni_3Al interfaces obtained from the present study at 0.0, 0.2, 2.0, and 3.0 dpa.

little change by 0.2 dpa, even though the γ′ layer is nearly fully disordered (see Figs. 2 and 3). Thus, the dissolution of the γ′ layer proceeds much more slowly than its disordering.

To quantify the rate of dissolution of the γ′ layer, we compute the mixing parameter Q on the basis of the concentration-position profiles discussed above. The square of the effective interdiffusion length, $D^{\text{eff}}t$, appearing in the numerator of the right-hand-side of Eq. (3) is obtained in accordance with the method developed by Zhang and Demkowicz[31] based on the Boltzmann-Matano analysis.[60] The value ϕF_D in the denominator of Eq. (2) is evaluated as the number of PKAs multiplied by the PKA energy and divided by the volume of the simulation cell.

The calculated mixing parameter displays a rapid reduction at low dose followed by a gradual decrease with increasing number of cascade events, as shown in Fig. 5. At low doses below approximately 0.15 dpa, the square of the effective interdiffusion length, $D^{\text{eff}}t$, grows nonlinearly with dose, which gives rise to large statistical errors in the mixing parameter. The average value of the mixing parameter is the highest, 220 Å^5 ± 12.7 eV^{-1}, and has the largest statistical error (standard deviation) at the first cascade. At the other extreme, the two layers in our model start to merge with one another around 0.5 dpa, causing the broadened concentration profiles from the two interfaces to overlap. The gradual decrease in mixing parameter at doses above 0.5 dpa is due to this overlap and may therefore be considered an artifact of the finite size of our simulation cell.

As described in Sec. IV, the experimental mixing parameter is determined under conditions where the interdiffusion coefficient is approximately constant. To make a comparison with the experimental value, we therefore assess the value of the mixing parameter in the present simulations using only doses between 0.15 and 0.5 dpa, for which the interdiffusion coefficient is

https://doi.org/10.1557/jmr.2014.377 Published online by Cambridge University Press

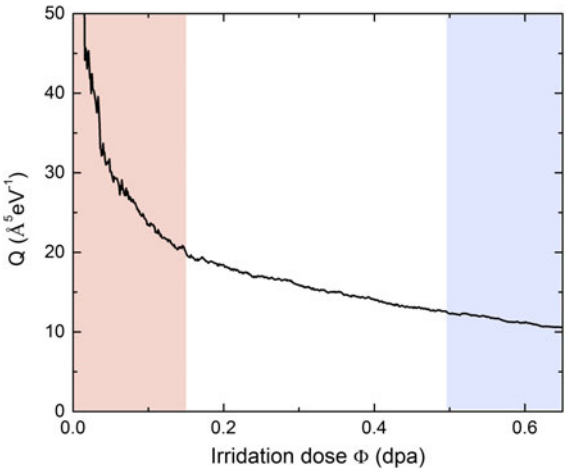


FIG. 5. Mixing parameter Q plotted as a function of dose in a Ni/Ni_3Al bilayer system obtained from the present study. Doses below ~0.15 dpa, where the square of the interdiffusion length grows nonlinearly with dose, are shaded red. Doses above 0.5 dpa, where the two interfaces begin to overlap, are shaded blue. We obtain the value of the mixing parameter in the dose range 0.15–0.5 dpa.

relatively steady with the two interfaces being well isolated from each other. Using this approach, we obtain Q = 12–20 Å^5 eV^{-1}. The standard deviation in Q is no larger than 0.65 Å^5 eV^{-1} in this range of doses.

To determine whether disordering affects dissolution, we performed simulations for the bilayer model starting with an initially disordered Ni_3Al layer with differing values of initial average order parameter. The mixing parameters obtained from these simulations are the same – to within statistical uncertainty – as those for the initially ordered Ni_3Al layer. This result demonstrates that disordering and mixing are decoupled processes in the absence of thermally activated diffusion.[17] We also assessed mixing and disordering in a bilayer model with a room temperature thermal equilibrium Al distribution, determined using the variance-constrained semi-grand-canonical Monte Carlo method.[61] In such a model, the whole system contains approximately 6.5 at.% more Al atoms than the idealized model shown in Fig. 1 and the Ni/Ni_3Al interface is not atomically sharp, even before irradiation. The values of the disordering efficiency and mixing parameter for this model are also within the statistical error of those obtained from the idealized model shown in Fig. 1.

IV. DISCUSSION

Several experimental studies provide quantitative measurements of the disordering efficiency and disordering rate of ordered γ' precipitates in Ni-base superalloys and model Ni–Al systems under ion irradiation.[5–8,11,33,34] Since our simulations do not model thermally activated diffusion, we compare them with room temperature experiments.

The stability of spherical γ' precipitates in Nimonic PE16 under irradiation with 300 keV Ni^+ ions was investigated by means of transmission electron microscopy (TEM) and atom probe tomography in Refs. 5 and 6. Nimonic PE 16 is a Ni-base superalloy containing Fe (34 at.%), Cr (16 at.%), Al (2.7 at.%), Ti (1.5 at.%), and Mo (2 at.%). Sun et al. recently studied the stability of γ' cuboidal precipitates in René N4 under irradiation with 3 MeV Ni^{3+} ions.[11] René N4 is a Ni-base superalloy whose composition is Cr (15 at.%), Co (10 at.%), W (2.6 at.%), Ta (2.1 at.%), Al (12.4 at.%), Ti (5.8 at.%), Mo (1.2 at.%), and Hf (0.67 at.%). The primary constituent elements of γ' precipitates in Nimonic PE16 and René N4 are Ni, Al, and Ti, which form nearly stoichiometric Ni_3(Al or Ti) intermetallic compounds in the $L1_2$ structure in both cases.

Müller[33] and Ewert et al.[7] independently reported the values of the disordering efficiency of pure, homogeneous Ni_3Al under 300 keV Ni^+ ion irradiation. Subsequently, de Almeida et al. also measured the disordering efficiency for pure, homogeneous Ni_3Al under irradiation with 6 MeV Ni^{2+} ions using TEM.[34] Schmitz et al. further measured the disordering efficiencies of spherical γ' precipitates in a Ni–Al binary alloy under 300 keV Ni^+ ion irradiation.[8] The disordering efficiencies and mixing parameters reported in the above references are summarized in Table I.

Experimental studies in Refs. 5–8, 11 report that γ' precipitates disorder at a comparably low dose within 0.1–0.2 dpa and then dissolve into the γ matrix at higher doses, which is in line with the findings of the present study (Fig. 3). The rapid reduction in chemical order reflects the narrow composition range of Ni_3(Al or Ti) compounds, which is readily destroyed by short-range atomic transport due to interdiffusion within TSs in the absence of thermal reordering.

The disordering efficiency of homogeneous Ni_3Al under 300 keV Ni^+ ion irradiation was independently reported by Müller[33] and Ewert et al.[7] to be $\varepsilon \approx 30$ dpa^{-1} and 16 dpa^{-1}, respectively. de Almeida et al.[34] pointed out that the difference in these values may arise from the fact that the authors of Refs. 33 and 7 used different displacement threshold energies in their fluence-to-dpa conversion. However, neither of these authors actually report the displacement threshold energies they used. The disordering efficiency subsequently reported by de Almeida et al. for homogeneous Ni_3Al is even lower, at $\varepsilon \approx 10$ dpa^{-1}.[34] These authors claim that the lower disordering rates they reported may be attributed to the larger incident ion energies they used: 6 MeV.[34] In irradiations using 3 MeV Ni^{3+} ions, Sun et al. estimated the disordering efficiency of cuboidal precipitates in René N4 to be 12 dpa^{-1}.[11] This value is close to that reported by de Almeida et al.[34] lending support to the view that

https://doi.org/10.1557/jmr.2014.377 Published online by Cambridge University Press

TABLE I. Comparison of the results of the present study with experimentally measured room temperature disordering efficiencies and mixing parameters.

	Material	Irradiation condition	Disordering efficiency ε (dpa^{-1})	Mixing parameter Q ($Å^5$ eV^{-1})
Ref. 8	5.0 nm and 9.2 nm spherical γ′ precipitates in model Ni–Al alloy	300 keV Ni^+ ion	54 and 26	N/A
Refs. 5 and 6	19 nm spherical γ′ precipitates in Nimonic PE16	300 keV Ni^+ ion	15	13.2
Ref. 11	450 nm γ′ precipitates in René N4	3 MeV Ni^{3+} ion	12	45
Ref. 33	Bulk Ni_3Al	300 keV Ni^+ ion	30	...
Ref. 7	Bulk Ni_3Al	300 keV Ni^+ ion	16	...
Ref. 34	Bulk Ni_3Al	6 MeV Ni^{2+} ion	10	...
Present simulations	Ni/Ni_3Al bilayer Bulk Ni_3Al	10 keV PKA energy	29 31	12–20

higher incident ion energies may lead to lower disordering efficiencies.[62]

Our simulations gave disordering efficiencies of ~29 dpa^{-1} and ~31 dpa^{-1} for the Ni/Ni_3Al bilayer and for single-crystal Ni_3Al, respectively. These values are in quantitative agreement with the work of Müller,[33] but a factor of 2–3 higher than the other experiments mentioned above. Because the above studies did not report the displacement threshold energies they used, it is not clear whether this discrepancy is due to differences in fluence-to-dpa conversions. However, it is to be expected that MD simulations will yield higher disordering efficiencies than experiments, even when identical threshold energies are used for at least two reasons. First, MD simulations only account for mixing induced by collision cascades and do not incorporate the effect of thermally assisted reordering, which decreases the apparent disordering rate. Although thermal diffusion in Ni_3Al is insignificant at room temperature,[17] a minor effect of re-ordering should be expected at any finite temperature. Second, MD simulations that use classical potentials do not take into account electronic processes. Therefore, these simulations may significantly underestimate thermal conductivities in metals, since they only model the lattice contribution to thermal conductivity and not the electronic contribution. Higher thermal conductivities give rise to more rapid quenching of thermal spike cores,[63] which in turn reduces the disordering rate.[30]

Schmitz et al.[8] measured disordering efficiency for bulk single-crystal Ni_3Al, spherical γ′ precipitates 9.2 nm in diameter, and ones with 5.0 nm diameter to be ε ~ 16 dpa^{-1}, 26 dpa^{-1}, and 54 dpa^{-1}, respectively. Their study appears to indicate that disordering efficiency systematically increases with increasing precipitate interface-to-volume ratio. However, the present study gives nearly identical disordering efficiencies for the Ni/Ni_3Al bilayer and for single-crystal Ni_3Al: ~29 dpa^{-1} and ~31 dpa^{-1}, respectively. Therefore, our results do not show any effect of interface-to-volume ratio on disordering efficiency.

The radiation-induced interdiffusion coefficient was determined to be $Q \approx 7.5 \times 10^{-14}$ $Å^2$ ps^{-1} for γ′ precipitates in Nimonic PE16 in Refs. 5 and 6. To deduce an experimental mixing parameter from this value, we used TRIM simulations[64] to compute the stopping power due to internuclear collisions for 300 keV Ni^+ ions impinging on Nimonic PE16. By averaging the nuclear stopping power over the penetration depth and using the reported ion flux of 0.8 mA m^{-2}, we assessed the experimental mixing parameter for this alloy to be 13.2 $Å^5$ eV^{-1}. This value lies at the lower end of the range of mixing parameters found in the present simulations: 12–20 $Å^5$ eV^{-1}. As in the case of disordering, the higher mixing parameters found in our simulations may be attributed to the minor amounts of thermally activated de-mixing in experiments and – more likely – to the longer lifetime of TSs due to the absence of electronic thermal conductivity in the MD simulations.

Sun et al. obtained a mixing parameter of 45 $Å^5$ eV^{-1} from measurements of the interdiffusion length at γ/γ′ interfaces in René N4 irradiated by 3 MeV Ni^{3+} ions,[11] i.e., much larger than that deduced from Refs. 5 and 6. This discrepancy may be due to a dependence of mixing parameters on the PKA energy. According to Bacon and Diaz de la Rubia,[57] mixing parameters increase approximately in proportion to the square root of the PKA energy. Therefore, in agreement with experimental results, a factor of ~3 difference in mixing parameters may be expected between the 3 MeV Ni^{3+} ion experiments of Sun et al. and the 300 keV Ni^+ ion experiments in Refs. 5 and 6. However, more work is required to confirm this deduction, since Bacon and Diaz de la Rubia only studied mixing for PKA energies up to 30 keV.[57]

Ni-base alloys such as René N4 and Nimonic PE16 contain solutes, defects, and microstructural features that are not represented in our simulations. Thus, the comparisons with the experimental data provided above should be viewed as qualitative. Nevertheless, the overall agreement between experiments and modeling predictions of disordering efficiency and mixing parameter at room temperature is remarkably good, lending cred-

https://doi.org/10.1557/jmr.2014.377 Published online by Cambridge University Press

ibility to the use of simple atomistic models to study complex mixing phenomena.

The assumption that thermally activated recovery processes may be neglected holds well for room temperature experiments in the Ni–Al system. At higher temperatures, however, thermally assisted reordering and de-mixing cannot be ignored.[6,8,17] In contrast to room temperature behavior, the disordering and dissolution of γ' precipitates at elevated temperatures appear no longer to be independent, but correlated.[6,8] The time scale required to model such processes exceeds that accessible in conventional MD. However, given that the crystal structure is preserved during disordering and dissolution, lattice kinetic Monte Carlo[18,65,66] or accelerated MD methods[67,68] may be useful to simulate these phenomena at higher temperatures.

ACKNOWLEDGMENTS

The authors are grateful to Daniel Schwen, Scott A. Skirlo, Cheng Sun, Wenshan Yu, and Liang Zhang for helpful discussions. This work was supported by the Laboratory Directed Research and Development program at Los Alamos National Laboratory under Project No. 20130118DR, under DOE Contract DE-AC52-06NA253.

REFERENCES

1. R.C. Reed: *The Superalloys: Fundamentals and Applications*, 1st ed. (Cambridge University Press, New York, NY, 2006).
2. R.S. Nelson, J.A. Hudson, and D.J. Mazey: Stability of precipitates in an irradiation environment. *J. Nucl. Mater.* **44**, 318 (1972).
3. D.I. Potter and H.A. Hoff: Irradiation effects on precipitation in γ/γ' Ni-Al alloys. *Acta Metall. Mater.* **24**, 1155 (1976).
4. D.I. Potter and D.G. Ryding: Precipitate coarsening, redistribution and renucleation during irradiation of Ni-6.35 wt% Al. *J. Nucl. Mater.* **71**, 14 (1977).
5. F. Bourdeau, E. Camus, C. Abromeit, and H. Wollenberger: Disordering and dissolution of γ' precipitates under ion irradiation. *Phys. Rev. B* **50**, 16205 (1994).
6. E. Camus, C. Abromeit, F. Bourdeau, N. Wanderka, and H. Wollenberger: Evolution of long-range order and composition for radiation-induced precipitate dissolution. *Phys. Rev. B* **54**, 3142 (1996).
7. J.C. Ewert, G. Schmitz, F. Harbsmeier, M. Uhrmacher, and F. Haider: Ion induced disordering and dissolution of Ni_3Al precipitates. *Appl. Phys. Lett.* **73**, 3363 (1998).
8. G. Schmitz, J.C. Ewert, F. Harbsmeier, M. Uhrmacher, and F. Haider: Phase stability of decomposed Ni-Al alloys under ion irradiation. *Phys. Rev. B* **63**, 224113 (2001).
9. H.K. Zhang, Z. Yao, C. Judge, and M. Griffiths: Microstructural evolution of CANDU spacer material Inconel X-750 under in situ ion irradiation. *J. Nucl. Mater.* **443**, 49 (2013).
10. H.K. Zhang, Z. Yao, M.A. Kirk, and M.R. Daymond: Stability of Ni_3(Al, Ti) gamma prime precipitates in a nickel-based superalloy Inconel X-750 under heavy ion irradiation. *Metall. Mater. Trans. A* **45A**, 3422 (2014).
11. C. Sun, K. Hatter, T. Pollock, Y. Wang, O. Anderoglu, J. Valdez, B.P. Uberuaga, R. DIckson, and S.A. Maloy: (2014, unpublished).
12. G. Martin: Phase-stability under irradiation: Ballistic effects. *Phys. Rev. B* **30**, 1424 (1984).
13. M. Przybylowicz, P. Bellon, and G. Martin: Modeling of ordered precipitates under irradiation: Dissolution regimes and interfacial width. *Proceedings of an International Conference on Solid: Solid Phase Transformations*, 1994, p. 999.
14. S. Matsumura, Y. Tanaka, S. Müller, and C. Abromeit: Formation of precipitates in an ordering alloy and their dissolution under irradiation. *J. Nucl. Mater.* **239**, 42 (1996).
15. G. Martin and P. Bellon: Driven Alloys. *Solid State Physics: Advances in Research and Applications*, **50**, 189 (1997).
16. C. Abromeit, E. Camus, and S. Matsumura: Modelling of dissolution profiles of ordered particles under irradiation. *J. Nucl. Mater.* **271**, 246 (1999).
17. J.C. Ewert and G. Schmitz: Reordering kinetics of ion-disordered Ni_3Al. *Eur. Phys. J. B* **17**, 391 (2000).
18. J. Ye, Y.H. Li, R. Averback, J.M. Zuo, and P. Bellon: Atomistic modeling of nanoscale patterning of $L1_2$ order induced by ion irradiation. *J. Appl. Phys.* **108**, 054302 (2010).
19. T. Diaz de la Rubia, A. Caro, and M. Spaczér: Kinetics of radiation-induced disordering of A_3B intermetallic compounds: A molecular-dynamics-simulation study. *Phys. Rev. B* **47**, 11483 (1993).
20. T. Diaz de la Rubia, A. Caro, M. Spaczér, G.A. Janaway, M.W. Guinan, and M. Victoria: Radiation-induced disordering and defect production in Cu_3Au and Ni_3Al studied by molecular-dynamics simulation. *Nucl. Instrum. Methods Phys. Res., Sect. B* **80–81**, 86 (1993).
21. M. Spaczér, A. Caro, M. Victoria, and T. Diaz de la Rubia: Computer-simulations of disordering kinetics in irradiated intermetallic compounds. *Phys. Rev. B* **50**, 13204 (1994).
22. M. Spaczér, A. Caro, M. Victoria, and T.D. de la Rubia: Computer-simulation of disordering kinetics in irradiated A_3B intermetallic compounds. *J. Nucl. Mater.* **212–215**, 164 (1994).
23. M. Spaczér, A. Caro, and M. Victoria: Evidence of amorphization in molecular-dynamics simulations on irradiated intermetallic NiAl. *Phys. Rev. B* **52**, 7171 (1995).
24. M. Spaczér, A. Caro, M. Victoria, and T.D. de la Rubia: Computer-simulations of disordering and amorphization kinetics in intermetallic compounds. *Nucl. Instrum. Methods Phys. Res., Sect. B* **102**, 81 (1995).
25. F. Gao and D.J. Bacon: Molecular-dynamics study of displacement cascades in Ni_3Al. 1. General features and defect production efficiency. *Philos. Mag. A* **71**, 43 (1995).
26. F. Gao and D.J. Bacon: Molecular-dynamics study of displacement cascades in Ni_3Al. 2. Kinetics, disordering and atomic mixing. *Philos. Mag. A* **71**, 65 (1995).
27. A. Almazouzi, M. Alurralde, M. Spaczer, and M. Victoria: Disordering in the Ni-Al system under low dose ion-irradiation: A computer simulation study. *Mat. Res. Soc. Symp. Proc.* **481**, 371 (1998).
28. F. Gao and D.J. Bacon: MD investigation of thermal spike effects on defect production and disordering by displacement cascades in Ni_3Al. *Microstructural Processes in Irradiated Materials* **540**, 661 (1999).
29. F. Gao and D.J. Bacon: Temperature effects on defect production and disordering by displacement cascades in Ni_3Al. *Mat. Res. Soc. Symp. Proc.* **80**, 1453 (2000).
30. S.A. Skirlo and M.J. Demkowicz: The role of thermal spike compactness in radiation-induced disordering and Frenkel pair production in Ni_3Al. *Scr. Mater.* **67**, 724 (2012).
31. L. Zhang and M.J. Demkowicz: Radiation-induced mixing between metals of low solid solubility. *Acta Mater.* **76**, 135 (2014).

https://doi.org/10.1557/jmr.2014.377 Published online by Cambridge University Press

32. R.S. Averback, D. Peak, and L.J. Thompson: Ion-beam mixing in pure and in immiscible copper bilayer systems. *Appl. Phys. A* **39**, 59 (1986).
33. S. Müller: Doctoral Thesis, Universität Berlin, Berlin, Germany, 1997.
34. P. de Almeida, R. Schäublin, A. Almazouzi, M. Victoria, and M. Döbeli: Quantitative long-range-order measurement and disordering efficiency estimation in ion-irradiated bulk Ni_3Al using cross-sectional conventional transmission electron microscopy. *Appl. Phys. Lett.* **77**, 2680 (2000).
35. A.J. Ardell and R.B. Nicholson: Coarsening of γ' in Ni-Al alloys. *J. Phys. Chem. Solids* **27**, 1793 (1966).
36. A.J. Ardell and R.B. Nicholson: On modulated structure of aged Ni-Al alloys. *Acta Met.* **14**, 1295 (1966).
37. A.J. Ardell: An application of theory of particle coarsening – γ' precipitate in Ni-Al alloys. *Acta Met.* **16**, 511 (1968).
38. M.S. Daw and M.I. Baskes: Semiempirical, quantum-mechanical calculation of hydrogen embrittlement in metals. *Phys. Rev. Lett.* **50**, 1285 (1983).
39. M.S. Daw and M.I. Baskes: Embedded-atom method: Derivation and application to impurities, surfaces, and other defects in metals. *Phys. Rev. B* **29**, 6443 (1984).
40. Y. Mishin: Atomistic modeling of the γ and γ'-phases of the Ni-Al system. *Acta Mater.* **52**, 1451 (2004).
41. J.F. Ziegler, J.P. Biersack, and U. Littmark: *The Stopping and Range of Ions in Solids* (Pergamon, New York, NY, 1985).
42. G.P. Purja Pun and Y. Mishin: Development of an interatomic potential for the Ni-Al system. *Philos. Mag.* **89**, 3245 (2009).
43. D. Schwen and A. Caro: (2014, unpublished).
44. M.P. Allen and D.J. Tildesley: *Computer Simulation of Liquids* (Oxford University Press, New York, NY, 1987).
45. P. de Almeida: *The Order-disorder Transformation and Microstructural Evolution in Nickel-Aluminium Intermetallics After Heavy-Ion Irradiation*. Doctoral Thesis, École Polytechnique Fédérale de Lausanne, Lausanne, Switzerland, 2000.
46. R.S. Averback: Atomic displacement processes in irradiated metals. *J. Nucl. Mater.* **216**, 49 (1994).
47. R.E. Stoller: Point defect survival and clustering fractions obtained from molecular dynamics simulations of high energy cascades. *J. Nucl. Mater.* **233–237**, 999 (1996).
48. K. Nordlund, M. Ghaly, R.S. Averback, and M. Caturla, T. Diaz de la Rubia and J. Tarus: Defect production in collision cascades in elemental semiconductors and fcc metals. *Phys. Rev. B* **57**, 7556 (1998).
49. D.J. Bacon, Y.N. Osetsky, R. Stoller, and R.E. Voskoboinikov: MD description of damage production in displacement cascades in copper and alpha-iron. *J. Nucl. Mater.* **323**, 152 (2003).
50. L. Malerba: Molecular dynamics simulation of displacement cascades in α-Fe: A critical review. *J. Nucl. Mater.* **351**, 28 (2006).
51. M.J. Norgett, M.T. Robinson, and I.M. Torrens: Proposed method of calculating displacement dose-rates. *Nucl. Eng. Des.* **33**, 50 (1975).
52. A. Caro, M. Victoria, and R.S. Averback: Threshold displacement and interstitial-atom formation energies in Ni_3Al. *J. Mater. Res.* **5**, 1409 (1990).
53. H. Zhu, R.S. Averback, and M. Nastasi: Molecular-dynamics simulations of a 10 keV cascade in β-NiAl. *Philos. Mag. A* **71**, 735 (1995).
54. S. Plimpton: Fast parallel algorithms for short-range molecular-dynamics. *J. Comput. Phys.* **117**, 1 (1995).
55. A. Stukowski: Structure identification methods for atomistic simulations of crystalline materials. *Modell. Simul. Mater. Sci. Eng.* **20**, 045021 (2012).
56. J.M. Cowley: An approximate theory of order in alloys. *Phys. Rev.* **77**, 669 (1950).
57. D.J. Bacon and T. Diaz de la Rubia: Molecular-dynamics computer-simulations of displacement cascades in metals. *J. Nucl. Mater.* **216**, 275 (1994).
58. L.R. Aronin: Radiation damage effects on order-disorder in nickel-manganese alloys. *J. Appl. Phys.* **25**, 344 (1954).
59. K.C. Russell: Phase-stability under irradiation. *Prog. Mater. Sci.* **28**(3–4), 229 (1984).
60. R.W. Balluffi, S.M. Allen, and W.C. Carter: *Kinetics of Materials* 1 (John Wiley and Sons, Inc., Hoboken, NJ, 2005).
61. B. Sadigh, P. Erhart, A. Stukowski, A. Caro, E. Martinez, and L. Zepeda-Ruiz: Scalable parallel Monte Carlo algorithm for atomistic simulations of precipitation in alloys. *Phys. Rev. B* **85**, 184203 (2012).
62. F.F. Komarov: *Ion Beam Modification of Metals* (Gordon & Breach Science, Philadelphia, PA, 1992).
63. C.P. Flynn and R.S. Averback: Electron-phonon interactions in energetic displacement cascades. *Phys. Rev. B* **38**, 7118 (1988).
64. J.F. Ziegler, M.D. Ziegler, and J.P. Biersack: SRIM – The stopping and range of ions in matter (2010). *Nucl. Instrum. Methods Phys. Res. B* **268**, 1818 (2010).
65. A.F. Voter: Introduction to the kinetic Monte Carlo method. *NATO Sci. Ser., II* **235**, 1 (2007).
66. E. Martínez, J. Marian, M.H. Kalos, and J.M. Perlado: Synchronous parallel kinetic Monte Carlo for continuum diffusion-reaction systems. *J. Comput. Phys.* **227**, 3804 (2008).
67. A.F. Voter, F. Montalenti, T.C. Germann, B.P. Uberuaga, and J.A. Sprague: Accelerated molecular dynamics methods. *Abstr. Pap. Am. Chem. Soc.* **223**, U500 (2002).
68. X.-M. Bai, A.F. Voter, R.G. Hoagland, M. Nastasi, and B.P. Uberuaga: Efficient annealing of radiation damage near grain boundaries via interstitial emission. *Science* **327**, 1631 (2010).

https://doi.org/10.1557/jmr.2014.377 Published online by Cambridge University Press